DOI 10.1007/s11182-020-01916-9

Russian Physics Journal, Vol. 62, No. 10, February, 2020 (Russian Original No. 10, October, 2019)

TWO-LEVEL NANOSTRUCTURAL STATES IN METALLIC BCC-MATERIALS AFTER HIGH-PRESSURE TORSION IN THE BRIDGMAN ANVILS

A. N. Tyumentsev,[1,2] I. A. Ditenberg,[1,2] I. V. Smirnov,[1,2] K. V. Grinyaev,[1,2] I. I. Sukhanov,[1,2] and A. S. Tsverova[2]

UDC 538.911; 548.4; 669-17; 620.186.8

The results of an electron-microscopy investigation of two-level nanostructural states (submicrocrystals, measuring about 100 nm in size with the inner nanostructure and nanocrystal size about 10 nm, and crystal lattice curvature of hundreds of deg/μm) formed in the specimens of unalloyed Ta *and* V *and* Mo–Re*-based alloys in the course of high-pressure torsion in the Bridgman anvils are generalized. A mechanism of their formation is proposed – quasiviscous motion of nanodipoles of partial disclinations, which is controlled by the flows of nonequilibrium point defects in the fields of high local pressure gradients. It is shown that the microstructure evolution with the increasing deformation degree consists in an increase in the volume fraction of a two-level nanostructural state, which results in a 3–4-fold increase in the microhardness of the deformed specimens, its maximum values being in the range $H\mu \approx (E/27–E/32)$. The principal physical factors and conditions of formation of these states upon plastic deformation of submicro- and nanocrystals are discussed.*

Keywords: BCC-metal materials, high-pressure torsion, electron microscopy, nanostructural states, partial disclination nanodipoles, point defects, quasiviscous deformation mode.

INTRODUCTION

According to [1–5], an important feature of microstructure evolution under severe plastic deformations of metallic materials in the Bridgman anvils is the formation of two-level states. These are submicrocrystals measuring tenths fractions of a micron with the inner (primarily nanobanded) structure with the size of nanocrystals from 5 to 20 nm, a dipole character of misorientations, and exceptionally high (hundreds of deg/μm) crystal lattice curvature. They are formed at the true logarithmic strains $e \geq 3$ in FCC-Ni and Cu specimens. Simultaneously with the formation of these states, a phenomenon of low-temperature dynamic recrystallization (DR) is developed [1, 2, 6]. It ensures a cyclic (DR $\rightarrow$ secondary fragmentation $\rightarrow$ DR $\rightarrow$…) character of structure formation (changes in defect density and dimensions of submicrocrystals) with a high inhomogeneity of the nanostructural state. Moreover, along with the areas of two-level nanostructural state there are defect-free nanograins of dynamic recrystallization and submicrocrystals with differing defect-density or crystal-curvature values. This inhomogeneity is observed in the entire range of continuing (at $e \geq 3$) plastic deformation.

A different (from nickel and copper) feature of the microstructure evolution in BCC-metal materials at $e > 3$ is the absence of dynamic recrystallization, which is likely to be due to considerably lower homological deformation temperatures. Under these conditions, the structural changes at the above-cited values of e are associated with the

[1]Institute of Strength Physics and Materials Science of the Siberian Branch of the Russian Academy of Sciences, Tomsk, Russia, e-mail: ditenberg_i@mail.ru; kvgrinyaev@inbox.ru; suhanii@mail.ru; [2]National Research Tomsk State University, Tomsk, Russia, e-mail: tyuments@phys.tsu.ru; smirnov_iv@bk.ru; tsverova@mail.ru.
Translated from Izvestiya Vysshikh Uchebnykh Zavedenii, Fizika, No. 10, pp. 95–105, October, 2019. Original article submitted August 7, 2019.

TABLE 1. Shear Deformation γ and True Logarithmic Strain e vs Number of Anvil Rotations and Distance to Disk Center

R, mm	e, γ	$N = 1$	$N = 3$	$N = 5$	$N = 7$	$N = 8$
0.5	γ	21	63	105	146	167
	e	3.0	4.1	4.7	5.0	5.1
1.5	γ	63	188	314	439	502
	e	4.1	5.2	5.8	6.1	6.2
3.5	γ	146	440	733	1025	1172
	e	5.0	6.1	6.6	6.9	7.1

evolution of the two-level nanostructural states. In the present work we generalize the results of an electron-microscopy investigation of the features of this evolution in the specimens of unalloyed Ta and V and Mo–Re-based alloys and analyze the mechanism of their formation. Also, regular patterns of microhardness variation as a function of the strain degree are studied.

EXPERIMENTAL MATEIALS AND PROCEDURE

The investigation is performed using the following alloys: V–4Ti–4Cr (V–4.36Cr–4.21Ti–0.013C– 0.011N–0.02O, wt. %) and Mo–47Re–0.4Zr (wt. %), and pure Ta specimens (99.99 %). An important characteristic of these materials is their high engineering plasticity. In a vanadium alloy, it is a capacity for practically unlimited value of plastic deformation by rolling at room temperature without any intermediate annealing [5]. In the alloys of the Mo–Re system, a similar characteristic is achieved due to the well-known rhenium effect [7]. These alloys, due to a simultaneous considerable increase in the strength and high melting temperature, are very useful model objects for investigating the behavior of large plastic deformations and formation of non-equilibrium nanostructural states under the conditions of minimal dislocation and diffusion activity.

Prior to deformation, Ta and V–4Ti–4Cr alloy were annealed for 1 h at $T = 1400$°C and Mo–47Re–0.4Zr alloy – at $T = 1600$°C. Their deformation in the Bridgman anvils was carried out at a pressure of ~7 GPa at room temperature. The specimens were shaped as disks with a thickness of $h = 0.2$ mm and a diameter of 8 mm. After deformation, the thickness (h_k) was 0.15 mm. The values of shear ($\gamma \approx 2\pi NR/h_k$ [8]) and true logarithmic ($e \approx \ln\gamma$) deformations versus the distance from the deformed disk center ($R = 0.5$–3.5 mm) and the number of anvil rotations (N) are listed in Table 1.

The electron microscopy investigation was performed in a Philips CM-30 STEM-TWIN (300 kV) electron microscope in thin foils cut in the cross sections perpendicular to the anvil planes. The specimens in in the cross sections parallel to the anvil planes were manufactured by the method of jet electropolishing in a 20 % solution of sulfuric acid in methanol. For the purpose of examination in the cross sections normal to the anvil plane, the 5×2×0.15 mm workpieces were electroplated with a ≈3 mm layer of copper, and then flat specimens were cut from them and mechanically ground to a thickness of about 100 μm. Further thinning of the specimens was carried out by sputtering argon ions on both sides at an accelerating voltage of 5 kV.

RESULTS AND DISCUSSION

Results of electron microscopy examination

Two-level structures begin forming in the submicrocrystalline (SMC) structural states with the crystal sizes about 100 nm at the values of true logarithmic strain $e \approx 3$. The defect substructure evolution for $e \leq 3$ was investigated in [3, 4]. It was shown that the fragmentation is mainly caused by the dislocational-disclinational mechanism (formation of substructures with high crystal curvature) and formation of the bands of noncrystallographic shear with crystal lattice reorientation.

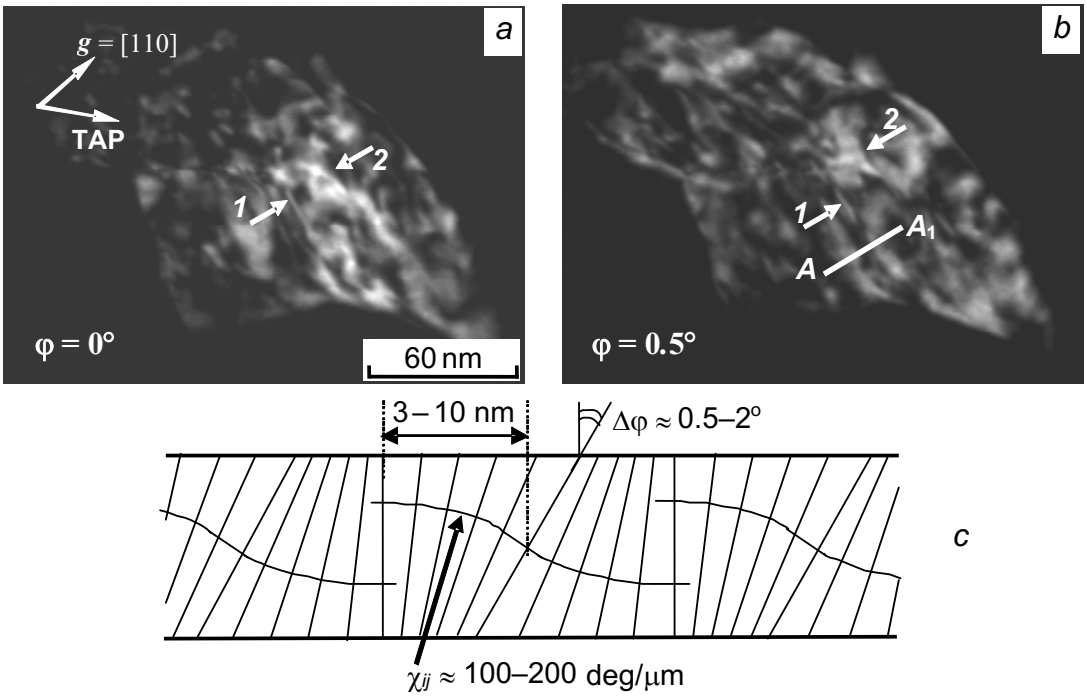

Fig. 1. Dark-field electron microscopy image of defect substructure of the V–4Ti–4Cr alloy submicrocrystal after high-pressure torsion in Bridgman anvils at $e \approx 4.1$ ($N = 3$, $R = 0.5$ mm) (*a*, *b*), φ – specimen tilt angle in the goniometer. Arrows *1* indicate a reorientation nanoband 2–3 nm in thickness, Arrows *2* – a discrete misorientation boundary, *c* – schematic of the defect substructure with dipole misorientations in the A–A_1 section. TAP – tilt axis projection.

An example of dark-field electron microscopy analysis of the nanostructural state in a vanadium alloy is given in Fig. 1. The electron-microscopy contrast characteristics (its periodic character, variations during specimen's tilting in the goniometer, typical banded (Fig. 1*b*, section A–A_1) and loop-like (Fig. 1*a*) extinction contour configurations) suggest the formation of misoriented structure with a dipole and multipole character of crystal lattice reorientation. The dimensions of the coherent scattering regions characterizing the typical dimensions of reoriented fragments (width of nanobands or radius of reorientation loops) are within the range from 2–3 (Arrows *1* in Fig. 1*a* and *b*) to 10 nm. The angles of reorientation between the fragments of the dipole and multipole structures do not generally exceed a few degrees.

During investigations of the extinction contour behavior, upon changing the specimen's orientation, various variants of crystal lattice reorientation were revealed inside the nanodipole or nanomultipole substructures and between their fragments:

– continuous variation in the orientation of the crystal lattice with high curvature, detected from the continuous extinction contour displacement after changing the foil orientation;

– discrete (low-angle) misorientation boundaries detected from discontinuation of the contour motion after tilting the specimen in the goniometer. One of such boundaries is indicated in Fig. 1*a* and *b* by Arrows *2*.

An investigation of the defect substructure features of the V–4Ti–4Cr alloy as a function of the strain degree demonstrated that the inner structure of submicrograins in the two-level nanostructural state is transformed at the values $e \geq 3$. As the degree of straining increases, the fraction of submicrograins, having two-level nanostructural state shown in Fig. 1, increases, and at $e \approx 6$ – this state becomes typical for the inner structure of submicrocrystals. Schematically, a fragment of this state is presented in Fig. 1*c*. This is an illustration of the fact in the case of a large value of the continuous component of the change in the fragment orientation in the dipole and multipole structures misoriented by

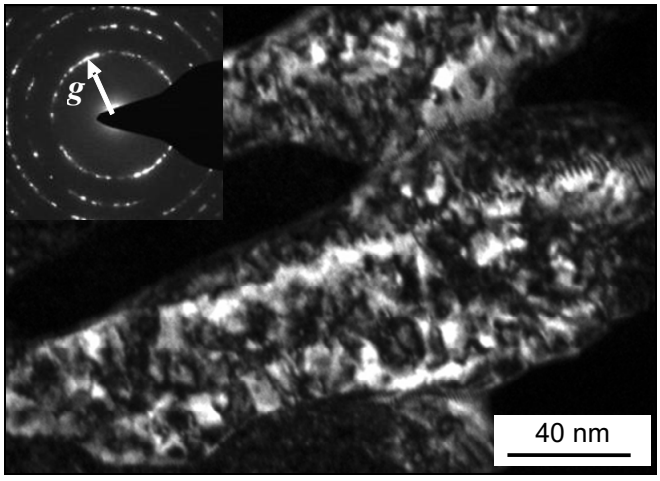

Fig. 2. Dark-field electron microscopy image of a two-level nanostructural state in a Ta specimen after its deformation in Bridgman anvils at $e \approx 4.1$ ($N = 3$, $R \approx 0.5$ mm).

1–2°, whose dimensions are less than 10 nm, the crystal lattice curvature can become as high as $\chi_{ij} \geq 100$–200 deg/μm. This is by an order of magnitude higher than that inside submicrocrystals before their transformation.

An example of a two-level nanostructural state in Ta is shown in Fig. 2. The dark-field electron microscopy image demonstrates an alternation of nanobands measuring about 15 nm in width and having dipole misorientations. The variable width (from ≈5 to 20 nm) of the extinction contours observed along the nanobands implies a complex misoriented inner structure of these nanobands characterized by high orientation gradients and availability of equiaxed nanofragments of the above-mentioned dimensions with continuous and discrete misorientations.

Figure 3 presents an example of the electron microscopy examination of the misorientations in a submicrocrystal of the Mo – 47% Re – 0.4% Zr alloy after high-pressure torsion at a pressure of ≈ 7 GPa in Bridgman anvils. An analysis of the dark-field images implies that two types of substructure can be singled out in this submicrocrystal.

1. Coherent scattering regions (misoriented fragments) with low-angle discrete and high continuous misorientations, whose dimensions are 30 (circled in Fig. 3*a* and *b*) to 10 nm (indicated by Arrows *1* in Fig. 3*b*)

2. Regions of nanobanded structure with dipole and multipole misorientations. The presence of multipole structure is evidenced by the loop-like extinction contour configurations (indicated by Arrows *2* in Fig. 3*b*). It is clear that the contour width, determining the dimensions of the characteristic nanobands or coherent scattering regions, is about 5 nm.

A dark-field analysis of the misorientations, which was performed in several operating reflections, has demonstrated that in the submicrocrystals with two-level fragmented structure the specimen tilt angles in the goniometer (φ), falling within the interval within which a relatively intensive dark-field electron microscopy contrast is observed to form irrespective of the operating reflection vector, are commonly as low as a few degrees. Therefore, the misorientation boundaries between the nanofragments are low-angle boundaries. In the submicrocrystal in Fig. 3, this interval is $\Delta\varphi \approx 4°$ for an operating reflection vector $\boldsymbol{g} = \langle 200 \rangle$ forming an angle $\beta \approx 56°$ with TAP. Furthermore, according to [9], the projection of the maximum possible misorientation angle between the nanofragments onto the operating reflection direction does not exceed $\boldsymbol{\theta} \approx \Delta\varphi \times \sin\beta \approx 3.3°$.

Based on the dark-field images in Fig. 3, in the nanofragments measuring tens of nanometers we can estimate the projection of the curvature tensor components $\chi(\boldsymbol{g})$ on the operating reflection direction $\boldsymbol{g}$. It is clear from Fig. 3 that in the ≈30 nm nanofragment marked by a circle the extinction contour for the specimen tilted in the goniometer by angle $\Delta\varphi \approx 1°$ is displaced by $\Delta r \approx 15$ nm (0.015 μm). For the crystallographic planes perpendicular to the electron wave vector or parallel to the foil plane, this projection would be determined by the formula $\chi(\boldsymbol{g}) \approx \Delta\varphi \times \sin\beta/(\Delta r)$ [9] and would be equal to $\chi(\boldsymbol{g}) \approx 60$ deg/μm.

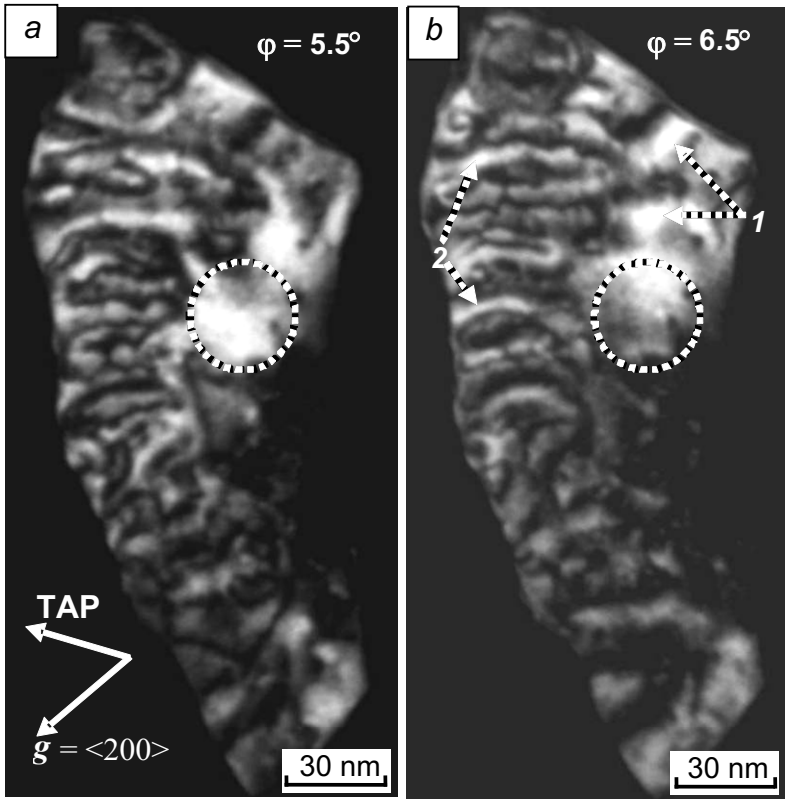

Fig. 3. Dark-field electron-microscopy image of the defect substructure of a submicrocrystal of the Mo–Re–Zr alloy after high-pressure torsion in Bridgman anvils at $e \approx 6.9$ ($N = 7$, $R \approx 3.5$ mm), φ – specimen tilt angle in a goniometer. TAP – tilt axis projection.

The crystal lattice curvature parameters in the region of nanobands, whose dimensions are a few nanometers, could not be determined in either the Mo–Re–Zr alloy in Fig. 3 (shown by Arrows *2*) or in the Ta specimens (Fig. 2). This is due to the fact that the extinction contour width in the dark-field images is by far larger than the aforementioned values, and the extinction contour motion in the course of the specimen orientation changes in the goniometer is degenerated into a change of their intensity. It is also impossible to measure the curvature of the planes parallel to the electron wave vector, since such a measurement assumes an availability of the information on the dimensions of the objects under study along this vector. In the structural states discussed in this work this measurement is practically impossible due to the complexity of the layered misoriented structure of submicrocrystals.

On the other hand, relying on the characteristic nanoband dimensions ($\Delta h \leq 10$ nm) and misorientation angles ($\Delta\varphi \approx 1$–$3°$), one can estimate the values of the local gradients of the crystal lattice orientation, which are made up of high continuous plus low-angle discrete misorientations. For the cited values of Δh and $\Delta\varphi$, these gradients ($\Delta\varphi/(\Delta h) \geq$ 100–300 deg/μm) can be comparable with the values of the elastic crystal lattice curvature observed in [10, 11] in the reorientation nanobands formed in the stage of formation of nanodipoles of partial disclinations in the zones of localization of elastic distortions. It is shown in [10, 11] that this curvature cannot be elastoplastic (dislocation induced), since the distance between the excessive same-sign dislocations have to exceed the characteristic dimensions of nanovolumes.

It follows from the results presented above that a common feature of the two-level nanostructural states in all the materials under consideration is the formation of misoriented nanostructures of the dipole type with high values of the elastic crystal lattice curvature. From our perspective, these features are consistently described using a quasiviscous mechanism of plastic deformation (by the flows of nonequilibrium point defects) described in [2, 10, 12] with

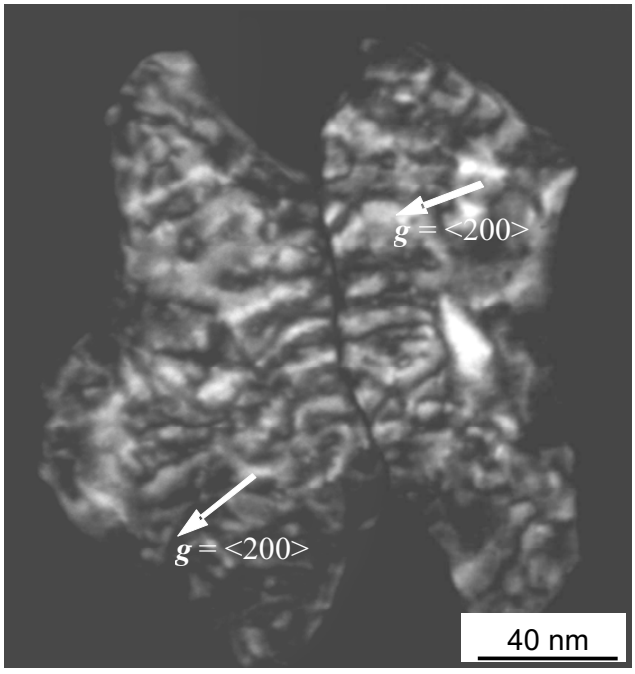

Fig. 4. Assembly of two dark-field images of the nanograins, separated by a large-angle boundary, after deformation by high-pressure torsion of the Mo–Re–Zr alloy in Bridgman anvils, $e \approx 6.9$ ($N = 7$, $R \approx 3.5$ mm).

participation of nanodipoles of partial disclinations (or noncrystallographic-shear dislocations), whose motion is solely determined by the inhomogeneous stress field character.

An illustration of the noncrystallographic character of development of two-level nanobands in the Mo–Re–Zr alloy is given in Fig. 4, presenting an assembly of one of the dark-field images of the nanograin shown in Fig. 3 and a neighboring grain. An electron diffraction analysis demonstrated that the {200}-type planes in these nanograins, which form the extinction contour contrast in Fig. 4, are misoriented by about 20°, in other words, the boundary between the nanograins is a large-angle boundary. Moreover, the orientation of nanograins with respect to the electron beam is such that the above-mentioned planes are simultaneously found in the reflecting position. In this case in the dark-field image in the $\boldsymbol{g}$ = <200> reflections formed by these planes it is possible to observe the behavior of nanobands with the two-level structure during their interaction with the nanograin boundary. It is clear in Fig. 4 that they penetrate into the neighboring grain practically without changing their propagation direction. Therefore, these directions are noncrystallographic and are exclusively determined by the geometry of the local field of deforming stresses.

It should also be noted that the absence in Fig. 4 of any visible effects of interaction between the nanobands and the nanograin boundary implies that this boundary does not present any essential obstacle for their propagation, which is a peculiarity of the situation and an indirect evidence of the quasiviscous plastic deformation mechanism during the formation of two-level nanostructural states.

In Ta and in the Mo–Re–Zr alloy, as well as in the V–4Ti–4Cr alloy, the first nanograins with the two-level nanostructural state are already observed after deformation at $e \approx 3$ ($N = 1$, $R \approx 0.5$ mm). A further increase in the deformation degree results in a gradual increase in the density of such grains. In the Mo–Re–Zr alloy, the above-mentioned state at a distance of $R \approx 0.5$ mm from the disc center fills the entire volume of the material for the number of anvil rotations $N = 3$ and $e \geq 4.1$. In the Ta specimens at $N = 1$ the two-level nanostructural state is revealed primarily in the periphery ($R \approx 3.5$ mm, $e \approx 5$) part of the specimens. Near the axis of torsion (for $R \approx 0.5$ mm and $e \approx 3$), the fraction of the substructure presented in Fig. 2 is relatively small. As the deformation degree is increased, this fraction gradually increases and at $N = 7$ the two-level nanostructural state occupies practically all of the material volume both in the periphery and central parts.

TABLE 2. Average Microhardness Values in Ta and Mo–Re and V-based Alloys vs. Number of Anvil Rotations and Distance from the Axis of Torsion

N	R, mm	γ	e	Hμ, GPa	Hμ
Ta, $E \approx 188$ GPa [13]					
Initial state (before deformation)				1.5	E/127
1	0.5	21	3.0	4.3	E/44
3	0.5	63	4.1	4.8	E/39
7	0.5	146	5.0	5.9	E/32
1	3.5	146	5.0	4.9	E/38
3	3.5	440	6.1	5.4	E/35
7	3.5	1026	6.9	5.9	E/32
Mo–47Re–0.4Zr, $E \approx 347$ GPa [14]					
Initial state (before deformation)				3.2	E/108
1	0.5	21	3.0	7.4	E/47
3	0.5	63	4.1	10.3	E/34
7	0.5	146	5.0	11.8	E/29
1	3.5	146	5.0	10.3	E/34
3	3.5	440	6.1	10.9	E/32
7	3.5	1026	6.9	9.3	E/37
1	0.5	21	3.0	7.4	E/47
V–4Ti–4Cr, $E \approx 347$ GPa [13]					
Initial state (before deformation)				1.5	E/85
1	0.5	21	3.0	3.2	E/40
5	0.5	104	4.6	3.7	E/34
1	3.5	146	5.0	3.4	E/37
5	3.5	730	6.6	4.8	E/26

The above-discussed microstructure evolution takes place in all materials under study inside the nanograins, whose dimensions and shapes vary insignificantly. It has to be underlined that the evolution is associated not only with a considerable (by about an order of magnitude) decrease in the dimensions of the misoriented nanofragments, but also with a multiple increase in the crystal lattice curvature inside these fragments.

Microhardness variation

The changes of microstructure discussed in the previous section are accompanied by a considerable increase in the microhardness. According to Table 2, a 3–4-fold increase of Hμ is observed in the course of deformation in all of the experimental alloys. In Ta (see also Fig. 5), near the axis of torsion ($R \approx 0.5$ mm) at $N = 1$, $\gamma \approx 20$ and $e \approx 3$ the average value of Hμ increases by about a factor of 3 (from 1.5 to 4.3 GPa). An increase in microhardness is observed when the deformation degree is increased with N. It reaches its maximum average value at $N = 7$ ($\gamma \approx 146$ and $e \approx 5$) and is found to be Hμ ≈ 5.9 GPa.

According to Fig. 5, the main feature of the Hμ variation is the large scatter of its values after deformation. To the fullest extent it is observed at low strain degrees. Near the axis of torsion after deformation at $\gamma \approx 20$ ($N = 1$) at the average value Hμ ≈ 4.3 GPa in different areas of the specimen it varies (Fig. 5, Curve *1*) in the range from about 3 to 5.4 GPa. In other words, the microhardness differences within these areas can be as high as ΔHμ ≈ 2.4 GPa. At the values of $\gamma \approx 63$ and 146 ($N = 3$ and 7) they decrease to ΔHμ ≈ 0.9 and 1.2 GPa, respectively.

Such a peculiar behavior is due to high defect-substructure inhomogeneity of the material. In the course of an electron microscopy examination this inhomogeneity is revealed as a presence of two qualitatively different

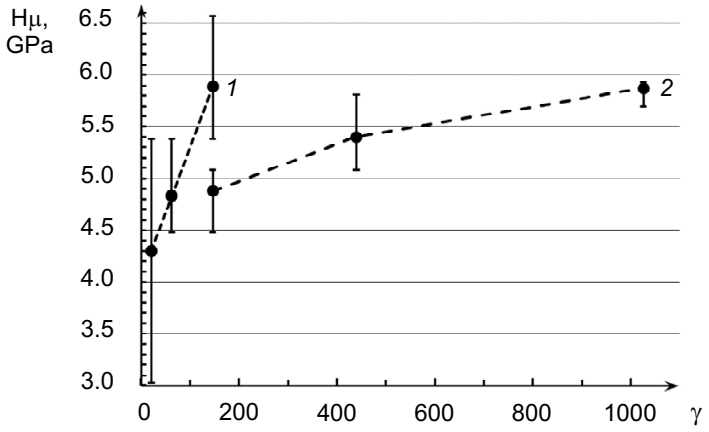

Fig. 5. Variation of microhardness in Ta specimens as a function of the deformation degree at the distances from the axis of torsion $R \approx 0.5$ mm (Curve *1*) and ≈3.5 mm (Curve *2*).

microstructure types: 1) submicrocrystalline state with the crystallite size about 100 nm, relatively low defect density inside them, and crystal lattice curvature of tens of deg/μm; 2) much more defective and, hence, higher strength two-level nanostructural state with by an order of magnitude finer (about 10 nm) crystallites and by an order of magnitude higher (hundreds of deg/μm) crystal lattice curvature. As the deformation degree is increased, this state gradually fills the material volume, decreasing the percentage of less strong fraction and the value of scatter in the strength of different microvolumes of the deformed specimens.

An important feature of the microhardness variation presented in Fig. 5 and Table 2 is a different behavior of the Hμ(γ) plots at different distances from the specimen center – a much faster microhardness growth (with increasing γ) near the axis of torsion (at $R \approx 0.5$ mm, see Table 2 and Curve *1* in Fig. 5). In this region, the average microhardness value Hμ ≈ 5.9 GPa is achieved at the shear strain degree γ ≈ 146. At a distance of $R \approx 3.5$ mm from the axis of torsion, a 7-fold increase of γ ≈ 1026 is necessary in order to produce a similar strengthening effect. A consequence of the above are large differences in the values of microhardness at the same value of the deformation degree γ ≈ 146: Hμ ≈ 5.9 GPa at $N = 7$ and $R \approx 0.5$ mm and Hμ ≈ 4.9 GPa at $N = 1$ and $R \approx 3.5$ mm, as well as close values of Hμ ≈ 4.8 and 4.9 GPa at different deformation degree γ ≈ 63 and 146, respectively.

The above-discussed behavior can be qualitatively estimated using the increments of the average microhardness values per unit shear strain (dHμ /dγ) in the central and periphery parts of the specimens. It is seen in Fig. 5 that at a distance of 0.5 mm from the axis of torsion within the experimental range of deformation degree (γ ≈ 21–146) its value is higher dHμ /dγ ≈ 12.7 MPa/γ. At a distance of 3.5 mm from the axis of torsion in the ranges of γ ≈ 146–440 and 440–1026 its values decrease to ≈1.8 and 0.8 MPa/γ, respectively.

For the analysis of this peculiar behavior it is important to take into consideration that an electron microscopy examination at different distances from the axis of torsion has revealed different character of the defect substructure evolution. At $R \approx 0.5$ mm, the volume fraction of the two-level nanostructural state increases with γ much faster than it does in the periphery region ($R \approx 3.5$ mm). As a result, in the former case it fills nearly the entire specimen volume at γ ≈ 146; while in the latter case – at γ ≈ 1026. It is clear that for the case of the above-mentioned ambiguous dependence of Hμ on the deformation degree, the character of microhardness variation is well correlated with the peculiar structural state, when the maximum values of microhardness both in the center and in the periphery of the deformed specimens correspond to the formation of more defective and stronger two-level nanostructural states in the entire volume of these specimens.

An increase in γ with the distance from the axis of torsion generally results in higher microhardness. In the present work, this is observed only at the plastic deformation values corresponding to the number of anvil rotations $N =$

1 and 3. At $N = 7$, in view of the effect discussed in this study that $\Delta H\mu/\gamma$ decreases with an increase in R, no such dependence is observed. The average values of $H\mu$ in the center and in the periphery of the deformed specimens are practically equal (5.9 GPa in Table 2). Moreover, the average microhardness value is observed at a distance of $R \approx 0.5$ mm from the axis of torsion. It is clear from Fig. 5 that in this region it is $H\mu \approx 6.6$ GPa; for $R \approx 3.5$ mm $H\mu \approx 5.9$ GPa.

The peculiar behavior described above can be accounted for by considering that an increase in the distance from the axis of torsion results in a respective increase not only in the strain degree but also strain rate. In the present study, by varying R from 0.5 to 3.5 mm the strain degree is increased by a factor of 7. The latter might result in a higher deformation temperature and more intensive processes of defect substructure relaxation. As it is known [15], under the conditions of high-pressure torsion this temperature increases by several hundred degrees.

In refractory Ta, the above-mentioned temperature increase cannot initiate such relaxation mechanisms as dynamic recrystallization in Al, Cu and Ni. In consistence with the electron-microscopy investigations, these would be the mechanisms of defect substructure and local internal stress relaxation in two-level nanostructural states, whose most important structural characteristics is a high (hundreds of deg/μm) crystal lattice curvature in the dipole-type reorientation nanobands measuring about 10 nm. According to [2, 10–12], the formation and subsequent evolution of these states can be described as the processes of nucleation and motion of partial disclination nanodipoles. Two stages of this process can be singled out: 1) generation and propagation of the zones of localized elastic distortion followed by the formation of localized shear and rotation nanobands; 2) plastic relaxation of the generated local internal stresses. The concept of a quasiviscous mode of deformation by the flows of nonequilibrium (generated during plastic deformation) defects in the fields of local pressure gradients underlie this relaxation.

The theoretical estimations made in [10, 12] demonstrated that due to a strong exponential dependence of the vacancy diffusion coefficient on temperature it is an important parameter determining the rate of plastic deformation under the conditions where the quasiviscous mode of deformation is realized. In particular, in nickel in the temperature interval from room temperature to 473 K an 100°C temperature increase can give rise to an increase in the local plastic shear rate in nanoband by 3–4 orders of magnitude.

These estimates demonstrate that under the conditions of a quasiviscous mechanism of deformation relatively low temperature gradients are sufficient for considerable differences to appear in the rates of the two-level nanostructural state relaxation intensity at different distances from the centers of the deformed specimens. They should be enough to enable its change during a transition from the center to the periphery of the specimens by less than 100°C. From our perspective, this is most probable considering the observed 7-fold difference in the plastic strain rates.

Thus under the conditions of deformation in the Bridgman anvils when analyzing the mechanisms of plastic deformation and variation of mechanical properties as a function of the distance from the axis of torsion, in addition to the dependence of the plastic deformation degree on this distance it is necessary to take into account possible formation of the temperature gradients determining the intensity of diffusion-controlled plastic relaxation processes in the forming nanocrystalline structures.

Similar features of microhardness variation are also observed in the Mo–Re–Zr alloy during its deformation in the Bridgman anvils (Table 2 and Fig. 6). After deformation at $N = 7$ the value of $H\mu$ in the specimen periphery (at $R =$ 3.5 mm, $\gamma \approx 1026$ and $e \approx 6.9$) is noticeably lower than in the central zone ($R = 0.5$ mm, $\gamma \approx 146$ and $e \approx 5$), while at $N =$ 5 these values are approximately equal. The temperature influence is likely to account for the nonmonotonic character of the microhardness dependence on the deformation degree (Fig. 6, Curve 2).

As it was noted above, the two-level nanostructural state in the Mo–Re–Zr alloy fills the entire specimen volumes at $N = 3$. At larger values of N no qualitative changes of the structural state were observed with an increase in the deformation degree up to the highest achieved values $e \approx 6.9$. It is important to note that this is accompanied by a slight increase or (at $N \geq 5$) a decrease in microhardness (Fig. 6). These results indicate that starting from a certain value of plastic deformation (at $N = 3$ in the specimen periphery and $N = 5$ in its central part) the defectiveness degree of the two-level nanostructural state does not practically change or (at $N \geq 5$ and $R \approx 3.5$ mm) decreases.

It is evident from the results listed in Table 2 that the maximum values of microhardness ($H\mu \approx 11.9$ GPa) are attained in the course of deformation in the Bridgman anvils in the Mo–Re–Zr-based alloy. In the Ta ($H\mu \approx 5.9$ GPa) and V–4Ti–4Cr alloy specimens ($H\mu \approx 4.8$ GPa) these values are at least twice lower. Their normalization with respect to the elastic moduli of the materials levels off these differences. In the Mo–Re alloys $H\mu \approx E/29$, in Ta $\approx E/32$ and in

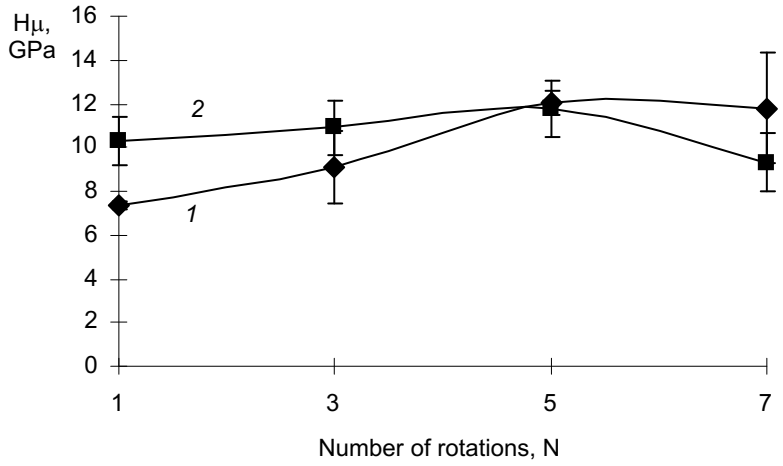

Fig. 6. Microhardness of the Mo–Re–Zr alloy as a function of the number of anvil rotations at the distances $R = 0.5$ (Curve *1*) and 3.5 mm (Curve *2*) from the specimen center.

the vanadium alloy it is $\approx E/26$. Therefore, the different absolute microhardness values in different materials are mainly associated with their different elastic moduli.

In all likelihood, after the formation of a two-level nanostructural state in the interval of deformation degrees γ from approximately 100 to 1000 ($e \approx 4$–7) plastic deformation can develop in a certain quasistationary evolution mode – at the unvaried microstructure and strength parameters. A good illustrative model for this evolution is the formation and plastic relaxation of nonequilibrium structural states with an elastic crystal lattice curvature of hundreds of deg/μm. In the case of partial disclination nanodipoles, these are the processes of their formation in the zones of elastic distortion localization [10, 11] and a subsequent relaxation of the nonequilibrium states assisted by the quasiviscous transfer mechanisms.

A decrease in the strength and hence the degree of microstructure defectiveness with an increase in the deformation degree, observed in the quasistationary mode above, suggests a possible quasiperiodic recurrence of the processes of formation and relaxation of the nonequilibrium nanocrystalline structures, which ensures very large (unlimited) plastic deformation values observed in the experiments. Note that this becomes possible in the two-level nanostructural state with a high density of nanobands measuring a few nanometers under the conditions of a quasiviscous deformation mechanism by the flows of nonequilibrium point defects. According to [2, 10], a high efficiency of this mechanism is determined by the following factors:

– high values of the local pressure gradients in the zones of retarded elastic shears and rotations or in the vicinity of the partial disclination nandipoles;

– short (a few nanometers) mass transfer lengths;

– high density of point defects.

It should be underlined that all these factors characterize nanocrystalline objects of a few nanometers in size.

SUMMARY

Two-level nanostructural states – submicrocrystals about 100 nm in size with the inner nanobanded structure, whose nanocrystals measure from 5 to 20 nm, dipole character of low-angle misorientations and crystal lattice curvature of hundreds of deg/μm have been revealed in the specimens of unalloyed Ta and V and Mo–Re-based alloys in the course of high-pressure torsion in the Bridgman anvils within the interval of true logarithmic strains $e \approx 3$–7 ($\gamma \approx 20$–

1000). It has been hypothesized that their formation occurs via the motion of partial disclination nanodipoles assisted by the quasiviscous deformation mode by the flows of nonequilibrium point defects in the field of local pressure gradients.

The evolution of microstructure with the increasing deformation degree consists in an increase of the volume fraction of the two-level nanostructural state and results in a ≈3–4-fold microhardness increase of the deformed specimens, its maximum value lying in the interval $H\mu \approx (E/27–E/32)$. A considerable decrease in the strain hardening intensity (value of $\Delta H\mu/\gamma$) has been observed with the increasing distance R from the axis of torsion. An assumption has been made that this results from an increase (with increasing R) in the plastic deformation rate resulting in a temperature increase and activation of the relaxation of the nanostructural states with high (hundreds of deg/μm) elastic crystal lattice curvature.

The electron microscopy investigations were supported by RSF (Project No. 17-19-01374); the mechanical properties were investigated within the Fundamental research program of the state academies of sciences for 2013–2020, research line III.23.

REFERENCES

1. I. A. Ditenberg, A. N. Tyumentsev, A. V. Korznikov, E. A. Korznikova, Phys. Mesomech., **16**, No. 3, 239–247 (2013).
2. A. N. Tyumentsev and I. A. Ditenberg, Fiz. Mezomekh., **14**, No. 3, 55–68 (2011).
3. I. A. Ditenberg, A. N. Tyumentsev, K. V. Grinyaev, *et al*., Tech. Phys., **56**, Iss. 6, 815–820 (2011).
4. I. A. Ditenberg, A. N. Tyumentsev, A. V. Korznikov, *et al*., The Physics of Metals and Metallography, **113**, No. 2, 160–169 (2012).
5. A. N. Tyumentsev, I. A. Ditenberg, A. S. Tsverova, *et al*., VANT, Ser.: Termoyad. Sint., **41**, Iss. 4, 48–64 (2018).
6. A. N. Tyumentsev, Yu. P. Pinzhin, I. A. Ditenberg, *et al.,* The Physics of Metals and Metallography, **96**, No. 4, 378–387 (2003).
7. V. I. Trefilov, Yu. V. Mil'man, and S. A. Firstov, Physical Foundations of the Strength of Refractory Metals [in Russian], Naukova Dumka, Kiev (1975).
8. N. A. Smirnova, V. I. Levit, V. I. Pilyugin, *et al*., Fiz. Met. Metalloved., **61**, No. 6, 1170–1177 (1986).
9. A. N. Tyumentsev, A. D. Korotaev, V. Ch. Gonchikov, and A. I. Olemskoy, Izv. Vyssh. Uchebn. Zaved. Fiz., **34**, No. 3, 244–252 (1991).
10. A. N. Tyumentsev, I. A. Ditenberg, A. D. Korotaev, and K. I. Denisov, Phys. Mesomech. **16,** No. 4, 319–334 (2013).
11. A. N. Tyumentsev, I. A. Ditenberg, I. I. Sukhanov, *et al*., Russ. Phys. J., **62**, No. 6, 962–971 (2019).
12. A. N. Tyumentsev, I. A. Ditenberg, I. I. Sukhanov, Russ. Phys. J., **62**, No. 8, 1313–1321 (2019).
13. J. P. Hirth and J. Lothe, Theory of Dislocations, McGraw-Hill, New York (1968).
14. E. M. Savitskii, M. A. Tylkina, and K. B. Povarova, Rhenium Alloys [in Russian], Nauka, Moscow (1965).
15. J. G. Li, M. Umemoto, Y. Todaka, *et al*., Rev. Adv. Mater. Sci., **18**, No. 6, 577–582 (2008).